RESIDENT SPACE OBJECT TRACK RECONSTRUCTION USING A MULTIRECEIVER RADAR SYSTEM

Luca Facchini[(1)]**, Marco Felice Montaruli**[(1)]**, Pierluigi Di Lizia**[(1)]**, Mauro Massari**[(1)]**, Giuseppe Pupillo**[(2)]**, Giovanni Naldi**[(2)]**, and Germano Bianchi**[(2)]

[(1)]*Department of Aerospace Science and Technology, Politecnico di Milano, Via G. La Masa 34, 20156 Milano, Italy:*
{luca.facchini, marcofelice.montaruli, pierluigi.dilizia, mauro.massari}@polimi.it
[(2)]*Istituto Nazionale di Astrofisica-Istituto di Radioastronomia, Via P. Gobetti 101, 40129 Bologna, Italy:*
{giuseppe.pupillo, giovanni.naldi, germano.bianchi}@inaf.it

ABSTRACT

In the framework of Space Surveillance and Tracking (SST), Italy contributes with the BIstatic RAdar for LEo Survey. BIRALES Field of View (FoV) can be populated with many independent beams, such that, during a passage, the beam illumination sequence enables the estimation of the angular path of the transiting object. A tailored signal processing and orbit determination procedure was developed in the past, but it turned out to be strongly affected by the signal quality. This work deals with the angular track estimation problem in a different way, through the application of MUltiple SIgnal Classification (MUSIC) algorithm. This approach grants the possibility to reconstruct the track without any need of slant range measurements. First, the methodology is applied to a synthetic dataset of LEO passages. Secondly, real data concerning observations of astronomical radio sources are processed. This is an intermediate step taken before moving to real data from debris passages.

Keywords: Radar; BIRALES; track reconstruction; multireceiver; debris.

1. INTRODUCTION

Over the last decades, particularly since the years '00s, the number of man-made objects in space has grown substantially, either intentionally or not. The two most affected regions are Low Earth Orbit (LEO) and Geostationary Orbit (GEO). Co-operative satellites represent only a small fraction of the total population, the majority is given by space debris, which include inactive satellites, rocket bodies, and fragments of all sizes [1]. Space debris pose a threat to the development of human activities in space as it leads to an increasing risk of possible in-orbit collisions, and for this reason they have called for the implementation of different mitigation strategies in order to guarantee safe operations. The goal of these measures is to possibly avoid the generation of new debris, as well as reducing their number. One of the actions that is being undertaken to meet these objectives is an international commitment in Space Surveillance and Tracking (SST), which involves the sharing of information between institutions and stakeholders. In Europe there are two programmes which deal with this topic: the European Space Agency (ESA) Space Situational Awareness (SSA) programme [2] and the European Space Surveillance and Tracking (EUSST) framework. The activities performed include conjunction analysis, collision risk assessment, fragmentation analysis and re-entry prediction [3] and they rely on the ability to detect and identify space objects with ground-based sensors. One of the most common sensors for observation of LEO debris, below 2000 km altitude, are radars. Some examples of european radar used for SST are TIRA, GESTRA, GRAVES, SATAM, S3TSR, MFDR and EISCAT [4, 5].

In Italy there is an on-going effort to contribute to the EUSST network with the BIstatic RAdar for LEo Survey (BIRALES) sensor [6]. In order to obtain accurate orbital state estimates, it is fundamental to be able to reconstruct the angular track of an object in an univocal way and with high precision, by employing a suitable processing technique. However, in the case of BIRALES, the process is hindered by the ambiguity of the receiver array. To achieve this task, a tailored algorithm was developed in the past based on a multibeam concept.

The goal of this paper is to investigate a method for the reconstruction of the angular profiles by exploiting a different concept, relying on signal processing techniques.

Initially the algorithm is tested on a synthetic dataset of 899 LEO passages from the NORAD catalogue. Then, the performances are assessed on real observations of some astronomical radio sources.

2. BIRALES SENSOR

BIRALES is a radar sensor operating in a bistatic configuration, with a baseline of 580 km. The transmitter (TX) is the Radio Frequency Transmitter (TRF), located at the Italian Joint Test Range of Salto di Quirra (Sardinia).
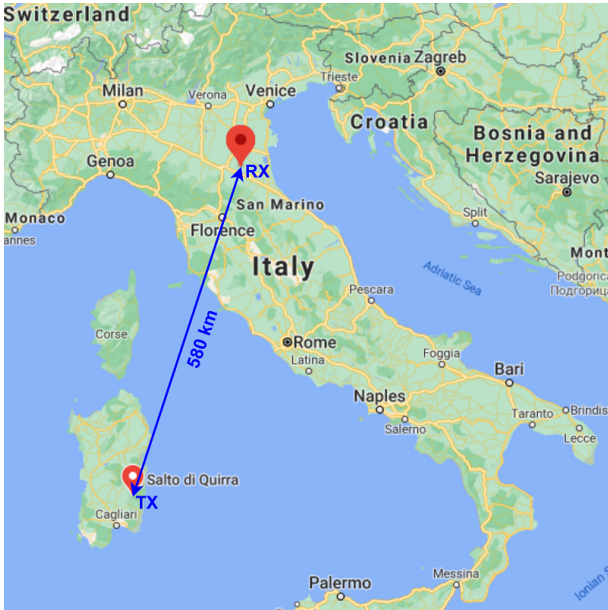
Figure 1: Location of BIRALES system.

Instead, the receiver (RX) is located at the Medicina Radio Astronomical Station (near Bologna), as shown in Fig. 1. The TX is a single parabolic antenna able to transmit a peak power of 10 kW in the frequency range 410-415 MHz and it has a beamwidth of 6 deg. The dish can be steered in both azimuth and elevation.

The RX is a portion of the Northern Cross Radio Telescope, which is one of the largest radio telescopes in the world. Fig. 2 shows BIRALES system, including both TX and RX. As it can be seen, the Northern Cross is T-shaped: one arm is arranged along the North-South (N-S) direction, the other is the East-West (E-W) one. Both arms can be mechanically pointed only in elevation, either in North pointing or South pointing configuration. The sensor operates in survey mode; thus, once the pointing strategy has been decided, the orientation of both TX and RX remains fixed throughout the observation and the tracking of the object is done electronically inside the field. As such, only objects which transit the local meridian of the receiver, and that can also be illuminated by the TX, are possibly observable. The E-W branch is a single antenna that is 564m long and 35m wide, but it is not used by BIRALES. The N-S arm is made of a linear array of 64 parallel antennas of cylindrical-parabolic shape, with a relative distance of 10 m and of size 23.5 m $\times$ 7.5 m each. BIRALES receiver is actually a section of the N-S arm that, at the present, includes 8 cylinders, but an extension is planned. Each cylinder contains 4 sensors arranged along the focal line, with a spacing of 5.67 m along E-W. Hence, the BIRALES RX consists of a planar array of 32 elements with a half-power beamwidth of 6.3 $\times$ 5.2 deg.

Different types of measurements are obtained by exploiting two different systems. The TX uses an umodulated continuous wave at 410.085 MHz, that allows to estimate the doppler shift (DS) and multiple signal-to-noise (SNR) ratio profiles. At the same time, the TRF can also provide slant range (SR) measurements by transmitting a pulse compressed chirp at 412.5 Mhz with a bandwidth of 4 MHz. Ranging is performed by processing the received signal with the matched filter and with coherent integration.

Currently the operative mode of the system is based on a multi-beam concept, as this kind of architecture allows to form several narrow beams in the receiver FoV. This is achieved by means of digital beamforming in the receiver back-end. The number and location of the beams can be decided by the user, but it is usually set to 32. An example of the resulting multibeam configuration is shown in Fig. 3.

By properly processing the aforementioned measurements, it is theoretically possible to infer the illumination sequence of the beams and, hence, to determine the trace of the transiting object. However, as the spacing between each element is longer than half wavelength in both E-W and N-S directions, multiple grating lobes are present for all beams. This results in possible ambiguities, as it is difficult to determine whether the illumination was due to the main lobes or due to the grating lobes.

Multibeam Orbit Determination Algorithm

The Multibeam Orbit Determination Algorithm (MODA) [7] was a tailored algorithm developed to tackle this issue. The algorithm is divided in three phases. The first one is the filtering phase, which takes as input the measured SNR profiles and the gain pattern of the multibeam system, and it aims at finding potential candidate sequences that are compliant with the maximum values of SNR of each beam. It starts with a cut of the detected SNR profiles, allowing to focus on a reduced number of illuminated beams. The candidates are generated by associating the SNR peaks to a certain number of gain peaks for each beam. Then the unfeasible candidates are filtered out, and the remaining ones are passed to a linear fitting in time, where the best candidate per cluster (gathering paths which cover a same region of the sensor FoV) is retained.

Next a refinement phase is carried out, which, for any beam, tries to associate all peaks in the SNR profile (not only the main one) to a gain peak which is responsible for the measurement. A second linear fit in time is performed and the best solution is selected according to an optimization process in a least square sense. Here, the measured SNR are matched against the predicted ones, and the available SR measures are used to compute the deterministic SNR necessary for the optimization. The best candidate outcoming from this step provides the rough estimate of the angular track, and it concludes the track reconstruction phase.

Finally, the third phase consists in a second optimization, in order to fit the orbital mean state (and possibly the Radar Cross Section) with the angular profile given at the end of the refinement phase and the SR and DS measurements. The final angular trace and the orbital state (in terms of mean state and covariance) are returned as output.

Although in synthetic data analysis this approach works properly, granting a successful track reconstruction in

Figure 2: BIRALES system. Left: Northern Cross (RX); right: TRF (TX).
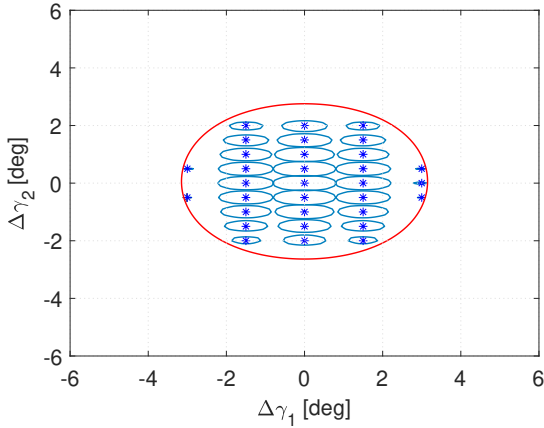

Figure 3: Multibeam configuration. In light blue: contour of the main lobe of each beam. Blue dots: peak of each beam. Red: contour of sensor element main lobe.

about 95% of the cases, in real scenarios the procedure turns out to be strongly affected by the signal quality. Hence, the process can either converge to a wrong solution or not converge at all.

3. TRACK RECONSTRUCTION METHOD FOR BIRALES

In order to overcome the issues mentioned beforehand, a method for track reconstruction based on modern signal processing techniques is investigated. In this way, the problem is treated as a parameter estimation problem rather than a least square optimization procedure. The received signal at each antenna can be written as

$$\boldsymbol{x}(t) = \boldsymbol{a}(\Delta\gamma_1, \Delta\gamma_2)s(t) + \boldsymbol{n}(t) \qquad (1)$$

where $\boldsymbol{a}(\Delta\gamma_1, \Delta\gamma_2)$ is the steering vector that depends on the angular deviations (azimuth and elevation) with respect to the RX Line of Sight (LoS). $s(t)$ is the temporal envelop of the signal and $\boldsymbol{n}$ is a complex noise (assumed to be Gaussian). Through a certain integration time, it is possible to compute the covariance matrix at a specific epoch

$$\boldsymbol{R_{xx}}(t) = \mathbb{E}\left\{\boldsymbol{x}\boldsymbol{x}^*\right\} \qquad (2)$$

Here it is assumed that the angles are time-varying during the total path, but that they remain approximately constant during the time interval when the signal is collected, which is reasonable if the integration time is short enough.

The problem is that of estimating the Direction of Arrival (DOA) $[\Delta\gamma_1, \Delta\gamma_2]$ from the signal $\boldsymbol{x}$ (or from $\boldsymbol{R_{xx}}$). For a radar array like BIRALES, different approaches exist such as beamforming-based methods, maximum likelihood and subspace methods. These estimators are formulated as an objective function that differ from each other according to hypothesis of the model and the assumed structure of the covariance matrix. Consequently, each technique results in a different accuracy and computational burden [8].

Given the need to be able to an obtain accurate solution in terms of track (and thus of orbital state), the choice was to employ a super-resolution technique. These methods are usually not employed for tracking the DOA because of the difficulty in real-time implementation. However, the approach is suitable for BIRALES, since no real-time implementation is needed and the whole data can be processed altogether after collecting the measurements. In particular it was decided to use the MUltiple SIgnal Classification (MUSIC) algorithm [9]. The rationale is that under normal operative conditions, the assumptions the method is based on are generally valid (i.e. knowing the number of objects that are passing through the FoV, and that the sources are uncorrelated), and the complexity is lower than other methods with comparable accuracy. In addition it is particularly suited to be implemented as an optimization procedure, which is useful if a coarse estimation of the location is known in advance.

The method exploits the spectral decomposition of the covariance matrix into the largest and smallest eigenvalues and corresponding eigenvectors, that is

$$\boldsymbol{R_{xx}} = \boldsymbol{U}\boldsymbol{\Lambda}\boldsymbol{U}^* \quad , \quad \boldsymbol{U} = [\,\boldsymbol{U_s} \;\; \boldsymbol{U_n}\,] \qquad (3)$$

and then the estimate of the location of source in the FoV is computed by solving the maximization of the function

$$J(\Delta\gamma_1, \Delta\gamma_2) = \frac{G(\Delta\gamma_1, \Delta\gamma_2)}{\boldsymbol{a}(\Delta\gamma_1, \Delta\gamma_2)^*\boldsymbol{U_n}\boldsymbol{U_n^*}\boldsymbol{a}(\Delta\gamma_1, \Delta\gamma_2)} \qquad (4)$$

The term $G(\boldsymbol{\Delta\gamma})$ represents the gain pattern of the array elements, and it is introduced to consider the directional properties of the sensors.

In this way it is theoretically possible to estimate the DOA at single epoch. In order to retrieve the angular track of the object clearly the process must be repeated with a suitable discretization in time.

A drawback arises from BIRALES array configuration: if one plots the spectrum in Eq. 4 at a particular epoch, it exhibits a main peak, but it also has some spurious peaks, with a spacing equal to $\Delta\gamma_1 \simeq \sin^{-1}(\frac{i}{d_x})$, $\Delta\gamma_2 = \sin^{-1}(\frac{j}{d_y})$, where d_x and d_y are the distances between receivers, measured in number of wavelengths, while i and j are integer indexes. These peaks all correspond to a possible solution. As an example, this is shown in Fig. 4.

The difference strengths of the peaks is given by the weights $G(\Delta\gamma_1, \Delta\gamma_2)$. In this case a criterion has to be selected in order to solve the possible ambiguity, and the solution can be still computed in a statistical sense.

The procedure is partly different depending on whether a prediction of the track of the object is known, by the user, thanks to orbital state prediction (provided by a TLE, for instance), or it is not. The overall scheme is shown in Fig.5, summarizing both cases.
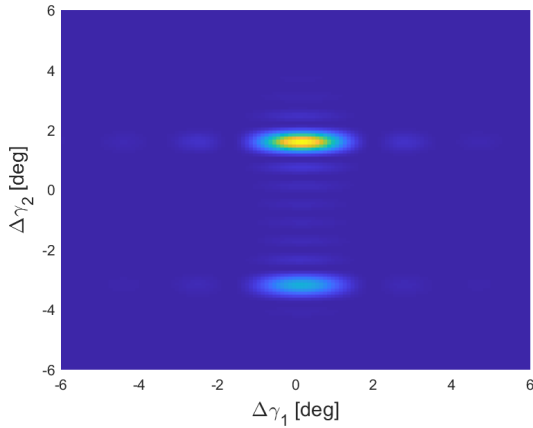

Figure 4: Spectrum at specific epoch.

3.1. Catalogued objects

The simplest case is when a prediction of the orbit is available. In this case the starting point is the transformation of the propagated orbit onto the sensor reference frame. This represents the reference track. The predicted track of the object can then be exploited to retrieve the track in a simple way:

1. At each observation epoch, find the local maximum of Eq. 4, using the initial guess $\Delta\gamma^0$ from the TLE

2. Perform a fit of the angular profile assuming a quadratic trend in time, t_0 being the first epoch of

observation:

$$\widehat{\Delta\gamma_1}(t) = a_2(t-t_0)^2 + a_1(t-t_0) + a_0 \quad (5)$$
$$\widehat{\Delta\gamma_2}(t) = b_2(t-t_0)^2 + b_1(t-t_0) + b_0 \quad (6)$$

At this point no further processing is necessary and the estimated angular profile is available, and it can be used for orbit determination.

3.2. Uncatalogued objects

In this case, it is necessary to select the peak which most likely represents the angular location of the source. In particular, the maximum peak is chosen.

The process is divided in the following steps:

1. For each epoch compute the DOA, that is the angular coordinates of the main peak, first with coarse grid. Later, starting from the coarse solution, a fine solution is found with an optimization procedure. In this way, by collecting the set of computed DOA (each associated to an epoch), this can result in possible multiple candidates tracks which are parallel to each other. An example is shown in Fig. 6.

2. A Density-based spatial clustering of applications with noise (DBSCAN) algorithm classifies points in the domain $\{t, \Delta\gamma\}$ in order to identify possible candidates, and it also filters out possible outliers. In this way, at first all points $\{t_i, \Delta\gamma_i\}$ are mapped into a cluster through an ID, called j, with $j \geq 0$. The resulting number of clusters is J, the total number of points in each cluster is N_j. The process is defined as

$$\{t_i, \Delta\gamma_i\}_{i=1}^{N_{obs}} \longrightarrow \{t_i^j, \Delta\gamma_i^j\}_{i=1}^{N_j} \quad , \quad 0 \leq j \leq J \quad (7)$$

where, in the notation $t_i^j, \Delta\gamma_i^j$, the subscript indicates the point from 1 to N_j belonging to the cluster j. The points that are labeled as noise (if any) belong to the cluster $j = 0$ and they are discarded.

3. It may happen that some clusters are associated to the same candidate track, although they may have been detected as different ones. This can occur, for example, due to spurious estimates at some epochs. An additional step is performed, aimed at aggregating the clusters into macro-clusters.

First, for each cluster j, the angular position is fitted by a linear path, with t_i^j the i-th epoch of each point belonging to j-th cluster:

$$\overline{\Delta\gamma_i^j}(t_i^j) = a_1^j\left(t_i^j - t_0\right) + a_0^j \quad (8)$$

Each candidate in theory has the same slope but different intercept. If some clusters have similar or same intercept, it means they represent the same track. Then, in order to aggregate the points into macro-clusters, a second clustering is performed
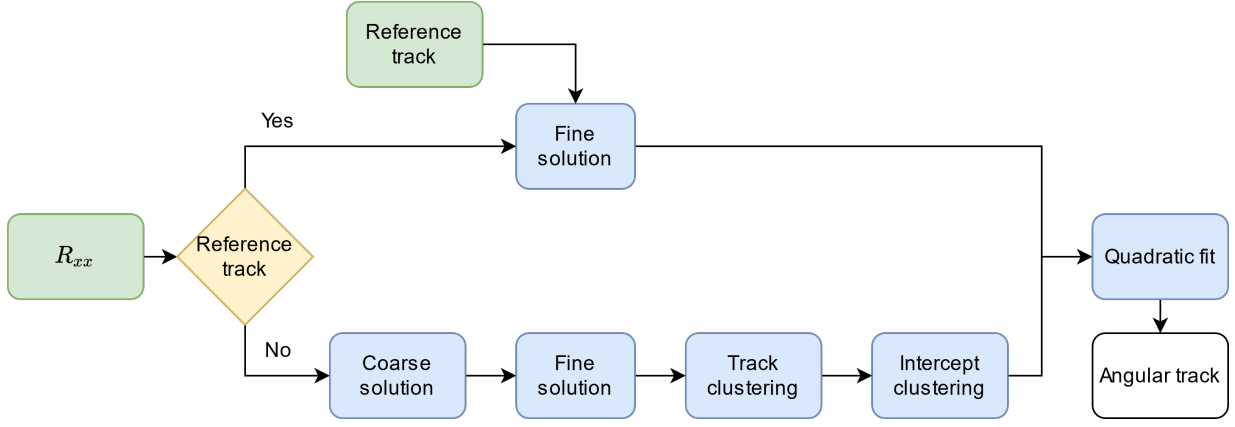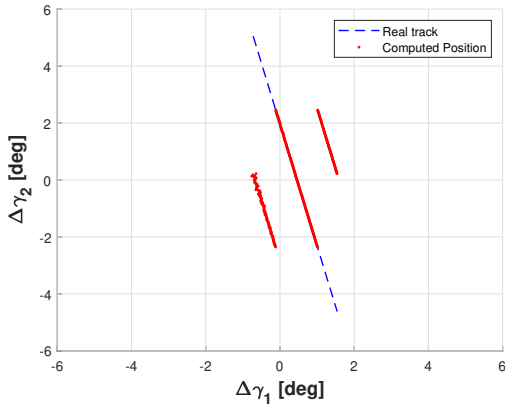
Figure 5: Processing scheme.

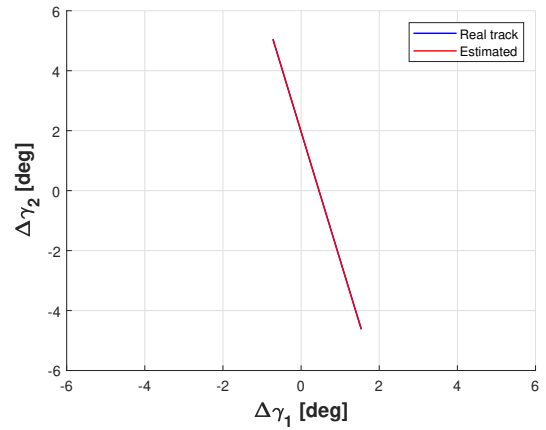Figure 6: Computed position resulting in multiple candidates.

Figure 7: Estimated track after processing.

considering as new dataset the set of intercepts $\{a_0^j\}$:

$$\{a_0^j\}_{j=1}^J \longrightarrow \{a_{0_v}^k\}_{v=1}^{N_k} \quad , \quad 1 \leq k \leq K \quad (9)$$

Given the indexes k of the second clustering and the indexes j of the first one, it is possible to associate each initial point $\{t_i, \Delta\gamma_i\}$ to the macro-cluster k

$$\{t_i, \Delta\gamma_i\} \longrightarrow \{t_i^k, \Delta\gamma_i^k\} \quad , \quad 1 \leq k \leq K \quad (10)$$

4. It is assumed that the cluster with most points represents the most likely track. Its corresponding points $\{t_i^M, \Delta\gamma_i^M\}$ are retrieved, and the complete angular profile is found with a quadratic fit, by considering all observation epochs (since the cluster is associated to a subset of the total observation instants).

The last point implicitly assumes that the track passes in the proximity of the center of the FoV. As we assume that the main peak given by weight of the element gain pattern represents the most probable location of the object, when this happens, on average the most populated candidate cluster is most likely correct. In this case, the portion of

the passage where the main peak does not coincide with the location of the object is a smaller fraction of the total angular track.

Figure 7 shows the resulting final track obtained from the DOA estimates reported in Fig. 6. It is possible to appreciate that there is a fine matching between the estimated angular profile and the exact one.

4. NUMERICAL SIMULATIONS

This section provides the statistical analysis performed with simulations, considering a synthetic dataset of 899 LEO passages taken from the NORAD catalogue.

All passages refer to objects observable by BIRALES in survey mode at 60 deg elevation (north-pointing). This is the configuration that is associated to the highest observation capability and passages are simulated such that they cover the entire receiver FoV.

For each object the track is projected onto the sensor reference frame, providing, for each epoch, the angular profile $[\Delta\gamma_1 \ \Delta\gamma_2]$ and the predicted SNR, according to relative geometry between the object and the ground stations

and the characteristics of the TX and RX. In the following analysis, these angular profiles are assumed to represent the exact object dynamics, and they are used as reference to assess the performances. The angular profiles and the SNR values are used to generate a set of synthetic covariance matrices, which are processed as in the previous section.

The index of merit for a single track k is the root mean square error (RMSE), i.e:

$$\text{RMSE}^k_{\Delta\gamma} = \sqrt{\sum_{i=0}^{N_{obs}-1} \frac{\left(\Delta\gamma(t_i) - \widehat{\Delta\gamma}(t_i)\right)^2}{N_{obs}}} \quad (11)$$

where N_{obs} is the total number of observation instants, $\Delta\gamma$ and $\widehat{\Delta\gamma}$ are the exact and estimated angular position, respectively.

The performances of the system are computed assuming both the case of catalogued and uncatalogued objects. In the first scenario, an uncertainty of the reference track is also added, to account for possible uncertainties and the intrinsic error of the propagation model. To this purpose the track prediction was perturbed with a random deviation, constant for all observation instants, assumed to be distributed with uniform probability density:

$$\boldsymbol{u}_{ref} = \boldsymbol{u}_{tle} + \overline{\delta u} \quad , \quad \overline{\delta u} \sim \mathcal{U}(-0.25°, 0.25°) \quad (12)$$

where a pessimistic maximum value of $\overline{\delta u}$ is used.

The results for the complete dataset are reported in Tab. 1, by considering the number of failures and the median root mean square error $\varepsilon^{50\%}_{\Delta\gamma}$ as indexes of merit of the statistical performances.

Table 1: Angular track estimation performance.

Case	Failures	$\varepsilon^{50\%}_{\Delta\gamma_1}$ (deg)	$\varepsilon^{50\%}_{\Delta\gamma_2}$ (deg)
Known objects	0	9.08e-04	5.08e-04
Unknown objects	15	1.64e-03	8.95e-04

As it can be seen, in case of catalogued objects, the track is always estimated correctly and very precisely. In case of uncatalogued objects, the criterion based on the most populated cluster provokes 15 failures, which correspond to a rate of 1.67% with this dataset, and the accuracy is comparable.

5. ANALYSIS OF REAL OBSERVATIONS

In the previous sections simulations were performed on synthetic data to determine the theoretical accuracy achievable in reconstructing the track. Before testing the algorithm on real LEO space debris passages, it turned out to be reasonable to focus on astronomical radio sources. Obviously these observations do not involve the complete BIRALES system, as there is no need for the TX, but they only focus on track reconstruction in the RX FoV. Such a real data analysis represents an intermediate step between synthetic data analysis and space debris passages related scenarios.

There are some differences between the echo of a LEO object and a radio source: observations of LEO passages last just few seconds, while an astronomic source takes at least several dozen minutes to transit through the FoV. This implies that the covariance matrices can be obtained using a higher number of temporal samples, whereas in the case of a LEO passage they need to be integrated for a lower amount of time. Nevertheless this approach still provides valuable insight on the expected performance in real scenario: for instance, the longer time of integration balances the lower SNR values expected with respect to LEO objects (for which peak values of 30 dB can be reached). Another potential issue, in debris observations, is the case of two or more objects entering the FoV at the same time, which can affect the measurements. By contrast, in the case of astronomical radio sources, this scenario is usually mitigated by the lengthy duration of observation, although debris and other interferences can still transit within the FoV throughout the duration of acquisition. Most importantly, another advantage in studying the performances of these sources is that their passages are precisely known with great accuracy. On the contrary, space debris passages prediction are always subject to not negligible uncertainties in the predicted angular track. Thus, this motivates the use of radio astronomical sources, as precise knowledge of a reference solution is fundamental for a validation procedure.

A dataset of 7 passages were available, referred to 4 different radio sources: Cassiopeia A, Taurus A, Cygnus A and Virgo A, hereafter referred to as Cas-A, Tau-A, Cyg-A and Vir-A, respectively. The celestial coordinates, RA and DEC in the J2000 frame are listed in Tab. 2. All observations were performed at 410.085 Mhz, that is equal to the umodulated continuous wave used by BIRALES for DS and SNR measurements. All passages were processed as if they were uncatalogued objects. The accuracy of all considered tracks, along with the dates of observation, are listed in Tab. 3. As an example, it is reported a passage of Cas-A (both exact and estimated) in Fig. 8.

Generally, the passages are estimated with appreciable accuracy, although with a lower precision than in case of synthetic tracks.

Table 2: J2000 coordinates of the radio sources.

Source Name	RA (deg)	DEC (deg)
Vir-A	187.7059	12.3911
Tau-A	83.6331	22.0145
Cas-A	350.8500	58.8150
Cyg-A	299.8682	40.7339

Table 3: Analyzed passages and resulting accuracy.

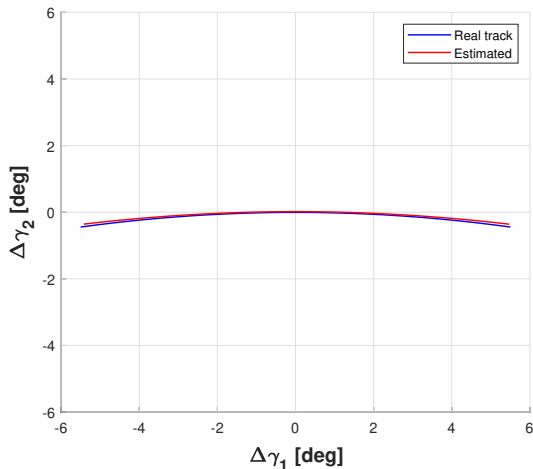| Source	Date	RMSE$_{\Delta\gamma_1}$ (deg)	RMSE$_{\Delta\gamma_2}$ (deg)
Vir-A	2019/12/04	7.530e-02	1.108e-01
Vir-A	2019/12/06	8.398e-02	1.121e-01
Tau-A	2019/12/05	6.555e-02	5.479e-02
Cas-A	2019/10/15	2.892e-02	2.454e-02
Cas-A	2020/03/24	3.113e-02	2.639e-02
Cas-A	2020/07/27	3.813e-02	4.749e-02
Cyg-A	2019/12/05	2.143e-02	3.735e-02

Figure 8: Angular track of Cas-A passage on 2020/07/27

6. DISCUSSION

The results of the previous sections on synthetic data and real observations are discussed in the following.

On synthetic simulations, as rule of thumb, the elevation component shows a greater accuracy. This result is consistent with what was obtained by the method previously employed, and it is explained by higher number of receivers in that direction. Unlike the MODA, failure cases behave differently, since track reconstruction success is mainly determined according to the variation of the angular distance from the LOS. One consequence of this property is that passages of uncatalogued objects which spend long time in the boundaries of the array visible region cannot be estimated correctly. In general, this affects mostly the elevation component (N-S), even though the E-W profile might be correct, since the extension of the unambiguous region is smaller in that direction. However, the occurrence of such cases appears to be quite low. Furthermore, at least on synthetic data, noise has little effect on the ability to reconstruct the track with this approach. Indeed, a high noise level influences the accuracy of the main peak solution just at a specific epoch. However track reconstruction involves many peaks, and the

influence is usually compensated by the whole angular profile, so that its effect becomes relevant for low SNR and/or significant deviations from the assumed model. Instead, the previous method involved a complex optimization procedure which was sensitive to the quality of the SNR profiles, and it was also reliant on SR. As a result, the algorithm was susceptible to convergence issues, worsening for higher noise levels of both SNR and SR and DS profiles. Finally, in case of catalogued objects, the method appears quite robust to errors in the angular track prediction.

Regarding the observations of radio sources, on average the accuracy tends to be two orders of magnitude worse than simulations. The factor most contributing to this loss in performance is a certain bias in the estimated profiles, which gives rise to the resulting lower RMSE. As a general trend, this is about 0.05 deg at the time of transit on the local meridian, and it increases farther from the LoS, reaching a maximum of about 0.25 deg. This effect is particularly relevant along the $\Delta\gamma_2$ direction and, as a result, a greater accuracy is obtained in the $\Delta\gamma_1$ direction, contrary to what happens in numerical simulations.

The main possible reasons contributing to this loss in performances are probably a combination of different factors: an inaccurate calibration of the system, which does not account for possible instrumental direction dependent effects and cross coupling, possible discrepancies between the assumed model and array properties and the actual ones, inaccurate pointing and lower SNR at the boundaries of the FoV.

Nevertheless the results are acceptable and promising, and they encourage the applicability of this processing technique.

7. CONCLUSIONS

The problem of track reconstruction of space objects is of utmost importance for accurate orbit determination. This issue is particularly problematic for BIRALES sensor because of the intrinsic ambiguity of the receiver array. This paper presented a new processing scheme of the system which relies on modern estimation techniques, and its achievable performances in terms of track estimation accuracy. The performances were first assessed through numerical simulations, starting from a synthetic dataset of LEO passages that are observable considering the bistatic geometry and interest the entire receiver FoV. The preliminary analysis highlighted that the track of most objects can be estimated correctly with high accuracy. In future works the processing scheme will be applied on a more comprehensive dataset. It will also modified to possibly reduce even further the failure rate, and it will be extended to track multiple objects at the same time.

Next, the algorithm was tested on the observations of some radio source passages. The results showed that the performances are lower than numerical simulations due to biases in the estimation, but it is expected to improve for debris passages with a high SNR and with a better calibration of the system. Overall the results are

promising, and future observations will be performed. The overall accuracy in terms of orbital state estimation will also be analyzed on real observations.

ACKNOWLEDGMENTS

REFERENCES

1. ESA Space Debris Office (2020), ESA's Annual Space Environment Report, techreport European Space Agency.

2. ESA SSA Programme overview, https://www.esa.int/Safety_Security/SSA_Programme_overview.

3. EU Space Surveillance and Tracking, https://www.eusst.eu/about-us/.

4. P. Faucher, R. Peldszus, A. Gravier (2019). Operational Space Surveillance and Tracking in Europe. In *1st International Orbital Debris Conference (IOC)*.

5. J. Vierinen, D. Kastinen, J. Markkanen, T. Grydeland, J. Kero, A. Horstmann, S. Hesselbach, C. Kebschull, E. Røynestad, and H. Krag (2019). 2018 beam-park observations of space debris with the EISCAT radars. In *1st NEO and Debris Detection Conference*.

6. G. Bianchi, C. Bortolotti, M. Roma, G. Pupillo, G. Naldi, L. Lama, F. Perini, M. Schiaffino, A. Maccaferri, A. Mattana, A. Podda, S. Casu, F. Protopapa, A. Coppola, P. Di Lizia, G. Purpura, M. Massari, M. F. Montaruli, T. Pisanu, L. Schirru, E. Urru (2020). Exploration of an innovative ranging method for bistatic radar, applied in LEO Space Debris surveying and tracking. In *71st International Astronautical Congress (IAC)*.

7. M. Losacco, P. Di Lizia, M. Massari, G. Naldi, G. Pupillo, G. Bianchi, J. Siminski (2020). Initial orbit determination with the multibeam radar sensor BIRALES. *Acta Astronautica*, 167:374-390.

8. H. Krim, M. Viberg (1196). Two decades of array signal processing research. *IEEE Signal Processing Magazine*, 13(4):67–94.

9. R. Schmidt (1986). Multiple emitter location and signal parameter estimation. *IEEE Transactions on Antennas and Propagation*, 34(3):276-280.